**RESEARCH ARTICLE**

# Oscillatory expression of Hes1 regulates cell proliferation and neuronal differentiation in the embryonic brain

Shohei Ochi[1,2], Yui Imaizumi[1,3], Hiromi Shimojo[1,6,*], Hitoshi Miyachi[1] and Ryoichiro Kageyama[1,2,4,5,*]

## ABSTRACT

The expression of the transcriptional repressor Hes1 oscillates in many cell types, including neural progenitor cells (NPCs), but the significance of Hes1 oscillations in development is not fully understood. To examine the effect of altered oscillatory dynamics of Hes1, we generated two types of *Hes1* knock-in mice, a shortened (type-1) and an elongated (type-2) *Hes1* gene, and examined their phenotypes focusing on neural development. Although both mutations affected Hes1 oscillations, the type-1 mutation dampened Hes1 oscillations more severely, resulting in much lower amplitudes. The average levels of Hes1 expression in type-1 mutant NPCs were also lower than in wild-type NPCs but similar to or slightly higher than those in *Hes1* heterozygous mutant mice, which exhibit no apparent defects. Whereas type-2 mutant mice were apparently normal, type-1 mutant mice displayed smaller brains than wild-type mice and upregulated proneural gene expression. Furthermore, proliferation of NPCs decreased and cell death increased in type-1 mutant embryos. When *Hes3* and *Hes5* were additionally deleted, neuronal differentiation was also accelerated, leading to microcephaly. Thus, robust Hes1 oscillations are required for maintenance and proliferation of NPCs and the normal timing of neurogenesis, thereby regulating brain morphogenesis.

KEY WORDS: Hes1, Neural development, Neural progenitor cell, Oscillation, Mouse

## INTRODUCTION

Many gene activities are oscillatory, and oscillatory expression regulates cellular activities (Levine et al., 2013; Purvis and Lahav, 2013; Isomura and Kageyama, 2014; Johnson and Toettcher, 2019). For example, the transcription factor NF-κB exhibits nuclear-cytoplasmic shuttling upon activation of this pathway and induces downstream gene expression differently depending on the shuttling frequencies (Hoffmann et al., 2002; Nelson et al., 2004; Ashall et al., 2009). Similarly, phosphorylated ERK (pERK) levels are pulsatile upon activation, and pulsatile but not sustained induction of pERK is important for cell proliferation rates (Albeck et al., 2013; Aoki et al., 2013). Another example is the somite segmentation clock gene *Hes7*, which exhibits oscillatory expression with ∼2-h periodicity in the mouse presomitic mesoderm; each cycle of *Hes7*

oscillation leads to formation of a bilateral pair of somites (Bessho et al., 2001; Pourquié, 2011; Oates et al., 2012). Hes7 represses its own expression by directly binding to the *Hes7* promoter, resulting in its oscillatory expression (Bessho et al., 2003). When *Hes7* expression is absent or sustained, all somites are severely fused (Bessho et al., 2001; Takashima et al., 2011), and an increase in the frequency of Hes7 oscillations accelerates somite formation (Harima et al., 2013), indicating that *Hes7* oscillations regulate the pace of somitogenesis. However, the significance of oscillatory expression in the development of other tissues still remains to be analyzed.

The transcriptional repressor Hes1 is expressed in an oscillatory manner by negative feedback, similar to *Hes7* oscillations, in many cell types, including neural progenitor cells (NPCs) (Jouve et al., 2000; Hirata et al., 2002; Shimojo et al., 2008; Bonev et al., 2012; Imayoshi et al., 2013; Chen et al., 2017). In the absence of *Hes1* and its related genes, NPCs are not properly maintained and prematurely differentiate into neurons without sufficient cell proliferation, resulting in microcephaly or anencephaly (Ishibashi et al., 1995; Hatakeyama et al., 2004; Sueda et al., 2019). However, sustained overexpression of Hes1 also inhibits proliferation of NPCs and enhances their quiescence (Baek et al., 2006), raising the possibility that oscillatory Hes1 expression is important for proliferation of NPCs. Hes1 oscillations periodically repress the expression of proneural genes, such as *Ascl1* and *Neurog2*, thereby driving their oscillatory expression in NPCs (Shimojo et al., 2008; Imayoshi et al., 2013). By contrast, in differentiating neurons, Hes1 expression disappears, and *Ascl1* or *Neurog2* expression becomes sustained, indicating that the expression dynamics of proneural genes are different between NPCs and differentiating neurons (Shimojo et al., 2008; Imayoshi et al., 2013). A previous study demonstrated that Ascl1 has dual opposing functions (Castro et al., 2011), and optogenetic analysis showed that Ascl1 induces neuronal differentiation when its expression is sustained, but activates the proliferation of NPCs when its expression is oscillatory (Imayoshi et al., 2013). These results suggest that the oscillatory expression of proneural factors, which normally depends on Hes1 oscillations, is important for efficient proliferation of NPCs (Imayoshi and Kageyama, 2014).

Despite the above findings, the significance of Hes1 oscillations in development is still obscure. Although sustained overexpression of Hes1 inhibits proliferation of NPCs, it is not clear which is more responsible for the inhibition of NPC proliferation – sustained (non-oscillatory) or high levels of Hes1 expression. To address this issue, it is important to examine whether dampened Hes1 oscillations, in the absence of increased expression levels, affect developmental processes. Mathematical modeling suggested that oscillatory expression is controlled by negative feedback with a delayed timing, which depends on transcriptional delays (the time required for production of mature mRNAs), and that changing such delays alters the oscillatory dynamics in the absence of increased expression levels (Lewis, 2003; Monk, 2003). We previously

[1]Institute for Frontier Life and Medical Sciences, Kyoto University, Shogoin-Kawahara, Sakyo-ku, Kyoto 606-8507, Japan. [2]Kyoto University Graduate School of Medicine, Kyoto 606-8501, Japan. [3]Graduate School of Pharmaceutical Sciences, The University of Tokyo, Tokyo 113-0033, Japan. [4]Kyoto University Graduate School of Biostudies, Kyoto 606-8501, Japan. [5]Institute for Integrated Cell-Material Sciences, Kyoto University, Kyoto 606-8507, Japan. [6]Graduate School of Frontier Biosciences, Osaka University, Suita, Osaka 565-0871, Japan.

*Authors for correspondence (hshimojo@fbs.osaka-u.ac.jp; rkageyam@infront.kyoto-u.ac.jp)

H.S., 0000-0001-5455-4218; R.K., 0000-0002-5985-1120

found that an important part of transcriptional delays is intronic delays (the time required for transcription and splicing of intronic sequences) (Takashima et al., 2011). Deletion of all three introns from the *Hes7* locus shortens the intronic delays, and under such a condition, Hes7 oscillation is dampened without an increase in its expression levels (Takashima et al., 2011). Similarly, removal of all intronic sequences from the Delta-like1 (*Dll1*) gene produced a shorter *Dll1* gene and decreased its transcriptional delay. By contrast, insertion of *Dll1* cDNA into the first *Dll1* exon while maintaining all exon and intron sequences produced a longer *Dll1* gene and increased its transcriptional delay (Shimojo et al., 2016), suggesting that the gene length also affects the transcriptional delay.

Therefore, to change the transcriptional delays, we decided to generate two types of *Hes1* mutant mice: a shorter version of *Hes1* with all three introns removed (type-1 mutant), and a longer version of *Hes1*, in which *Hes1* cDNA was inserted between the 5′UTR and the coding sequence (type-2 mutant). We then examined *Hes1* expression dynamics and developmental defects in these mutant mice, focusing on neural development.

## RESULTS

### Generation of *Hes1* type-1 and type-2 mutant mice

To examine the significance of *Hes1* oscillation in development, we tried to alter the *Hes1* expression dynamics. To this end, we first performed numerical simulations, using the same equations and parameter values to those of *Hes7* oscillations, because *Hes1* has similar oscillation dynamics to *Hes7* (Hirata et al., 2004; Takashima et al., 2011). This simulation suggested that altering the transcriptional delay ($T_m$; see Materials and Methods) would change the dynamics of Hes1 oscillations (Fig. S1). When the transcriptional delay was shortened compared with that of the wild type (Fig. S1A), oscillations were accelerated (faster oscillations) but dampened (Fig. S1B,C). On the other hand, when the transcriptional delay was lengthened, oscillations with a longer period continued (slower oscillations; Fig. S1D). We previously showed that the intronic delay and the gene length affect the transcriptional delay (Takashima et al., 2011; Harima et al., 2013; Shimojo et al., 2016). Therefore, we generated two types of *Hes1* mutants, a shorter version of *Hes1* with all three introns removed (type-1 mutant; Fig. 1A) and a longer version of *Hes1* in which the coding sequence with a stop codon of *Hes1* cDNA was inserted between the 5′UTR and the coding sequence in the first exon (type-2 mutant; Fig. 1B).

To determine whether type-1 and type-2 mutations change the transcriptional delay of *Hes1* expression compared with the wild-type control, we generated three reporters – the wild-type *Hes1* gene (control), the intronless *Hes1* gene (type-1 mutant) and the *Hes1* gene with *Hes1* cDNA knocked-in into the first exon (type-2 mutant) – each of which contained *Luc2* cDNA fused in-frame at the 5′ end of the coding region (Fig. S2A). We introduced each reporter into C2C12 myoblast cells and neural stem cells (NSCs) and activated the *Hes1* promoter with serum treatment to measure the expression kinetics of the *Hes1* reporters. Expression of the type-1 mutant reporter occurred ~13.5 min faster than the control in C2C12 cells and 3-12 min faster than the control in NSCs (Fig. S2B,C). By contrast, expression of the type-2 mutant reporter was ~5 min slower in C2C12 cells than the control but did not exhibit a significant difference in NSCs compared with the control (Fig. S2B,C), implying that the transcriptional delay was shorter in the *Hes1* type-1 mutant but longer or the same in the type-2 mutant cells compared with the control.

To generate *Hes1* type-1 mutant mice, a targeting vector containing *Hes1* cDNA and a neomycin expression cassette (pPGK-Neo-pA) was prepared (Fig. 1A). To generate *Hes1*

type-2 mutant mice, *Hes1* cDNA and pPGK-Neo-pA were inserted between the 5′UTR and the coding region of the first exon (Fig. 1B). Each targeting vector was introduced into mouse embryonic stem cells (ESCs) and homologous recombinants were obtained. These recombinants were used to make chimeric mice, which were then crossed with mice ubiquitously expressing flippase (FLP) to remove the neomycin expression cassette (Fig. 1A,B). Heterozygous mutant mice derived from the recombinant ESCs were born normally, and from these mice we generated homozygous mice (*Hes1* type-1 and type-2 mutant mice). Both *Hes1* type-1 and type-2 mutant mice were born at the Mendelian ratio and grew to fertile adults. We also confirmed that the expression continued in the downstream region of *Hes1* type-2 mutant NPCs (Fig. 1C).

### *Hes1* expression dynamics in the type-1 and type-2 mutant NPCs

To examine the *Hes1* expression dynamics of *Hes1* type-1 and type-2 mutants, we analyzed time-lapse imaging of the *Hes1* promoter-driven destabilized luciferase reporter (pHes1-Ub-luc; Fig. 2A), which monitors the endogenous *Hes1* expression (Fig. S3) (Masamizu et al., 2006). As previously described, the *Hes1* reporter exhibited oscillatory expression with a period of 173.5± 4.4 min in NPCs derived from wild-type mice (Fig. 2B,E,H,K,O, Fig. S4A). *Hes1* expression also oscillated in both *Hes1* type-1 and type-2 mutant NPCs (Fig. 2C,D,F,G,I,J,L,M, Fig. S4B,C). However, in *Hes1* type-1 mutant NPCs, the amplitude of the oscillation was much smaller (about 37% of the WT; Fig. 2N), and the period was slightly shorter (159.9±2.6 min; Fig. 2O). In *Hes1* type-2 mutant NPCs, the oscillation amplitude was smaller (about 62% of the wild type; Fig. 2N), but the period was slightly longer (187.0±4.3 min; Fig. 2O). These results indicated that Hes1 oscillations were severely dampened in type-1 mutant NPCs, whereas they were less affected in type-2 mutant NPCs. We previously found that *Hes1* oscillations in NPC cultures are very similar to those in brain slices (Shimojo et al., 2008), suggesting that *Hes1* oscillations are also affected in the intact brain of both types of mutants. In the type-2 mutant embryos, we did not find any significant defects in the developing nervous system (Fig. S5), but the type-1 mutant embryos displayed defects in neural development. Thus, we decided to examine the type-1 mutant mice in more detail.

Analyses of anti-Hes1 immunohistochemical staining in the developing nervous system demonstrated that Hes1 protein expression was variable and displayed a 'salt-and-pepper' pattern in wild-type NPCs (Fig. 3A-C), which might reflect oscillatory expression. In individual cells, there was a wide range of Hes1 protein levels in the wild-type cortex (Fig. 3B,C). By contrast, in *Hes1* type-1 homozygous mutant NPCs, Hes1 protein levels were less variable (Fig. 3A-C) and average levels were slightly reduced (Fig. 3D). This reduction in the average level was also confirmed by western blot analysis (Fig. 3E). Thus, *Hes1* type-1 mutant NPCs, in which the transcriptional delay of Hes1 expression was shortened, exhibited dampened oscillations without an increase in expression levels.

*In situ* hybridization analysis indicated that *Hes1* mRNA was slightly downregulated in *Hes1* type-1 homozygous mutant embryos, compared with the wild type (Fig. 3F). Quantification analysis revealed that *Hes1* mRNA levels were ~40% lower at embryonic day (E) 12.5 in the *Hes1* type-1 mutant brain than in the wild type (Fig. 3H). By contrast, *Hes3* and *Hes5* mRNAs were slightly upregulated in the *Hes1* type-1 homozygous mutant brain at E12.5, compared with the wild type (Fig. 3G,H), suggesting that *Hes3* and *Hes5* upregulation may compensate for *Hes1*
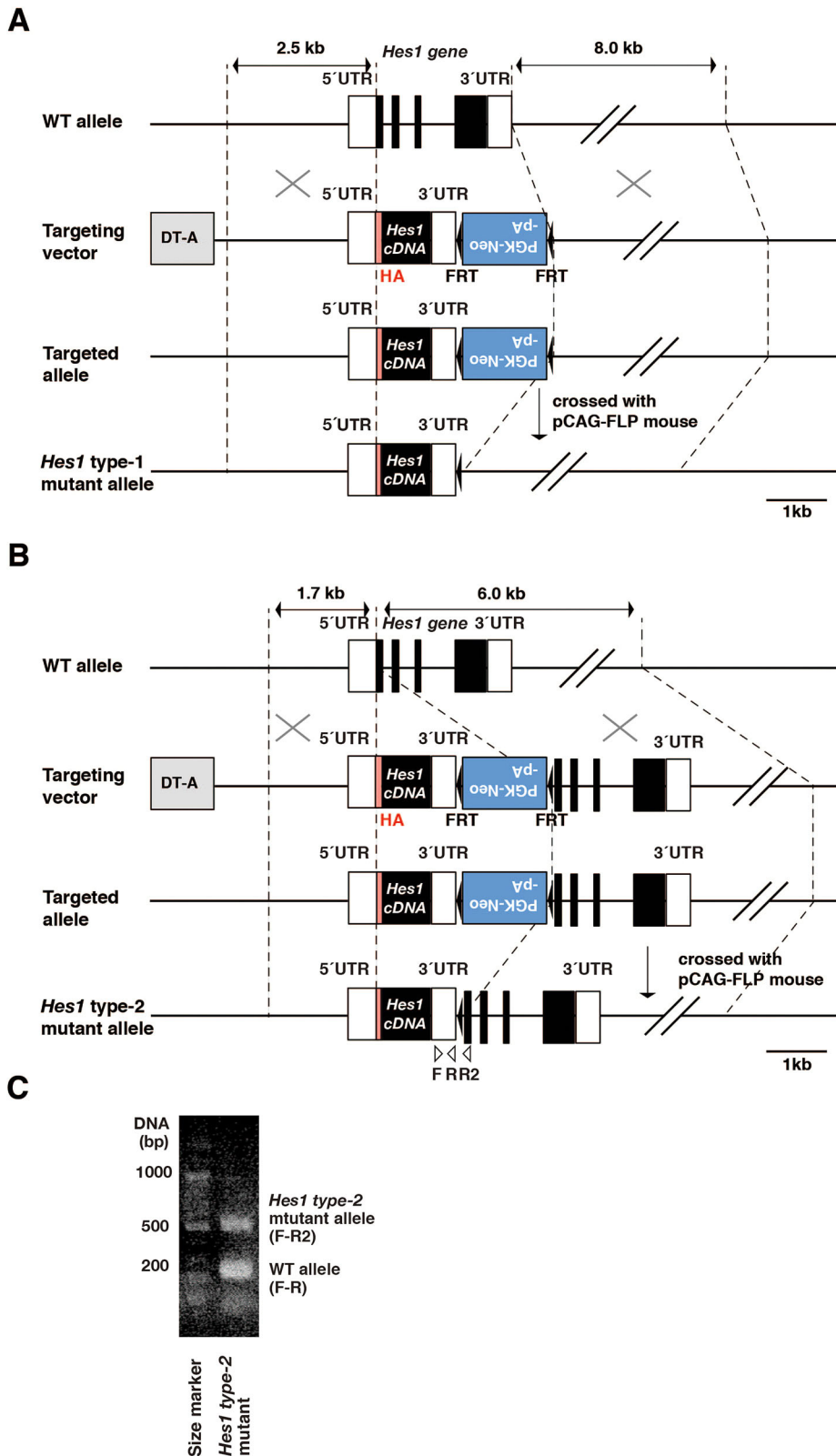
Fig. 1. Generation of *Hes1* type-1 and type-2 mutant mice. (A,B) Strategies for generating *Hes1* type-1 (A) and type-2 (B) mutant mice. Black and white boxes indicate coding and non-coding regions of *Hes1*, respectively. The targeting vector was introduced into mouse ESCs, and heterozygous mutant mice were obtained. Then, a neomycin resistance gene cassette flanked by FRT sites was removed by crossing with pCAG-FLP mice. White triangles in B indicate the positions of primers. (C) PCR analysis of *Hes1* gene transcription of *Hes1* type-2 mutant mice using the primers indicated in B. WT, wild type.

downregulation in the *Hes1* type-1 mutant brain at E12.5. However, at E14.5, although the Notch ligand gene *Dll1* was slightly upregulated, *Hes1*, *Hes3* and *Hes5* mRNA levels were not significantly different in *Hes1* type-1 mutant compared with wild-type embryos (Fig. 3H), suggesting that Hes gene expression became normalized at later stages of development.

## Defects of neural development in *Hes1* type-1 homozygous mutant embryos

To explore the possible effects of altered *Hes1* expression dynamics on development, we first examined the neural development of *Hes1* type-1 mutant mice. *Hes1* type-1 mutant mice had smaller whole bodies than wild type at E12.5 but recovered afterwards (Fig. 4A,B).
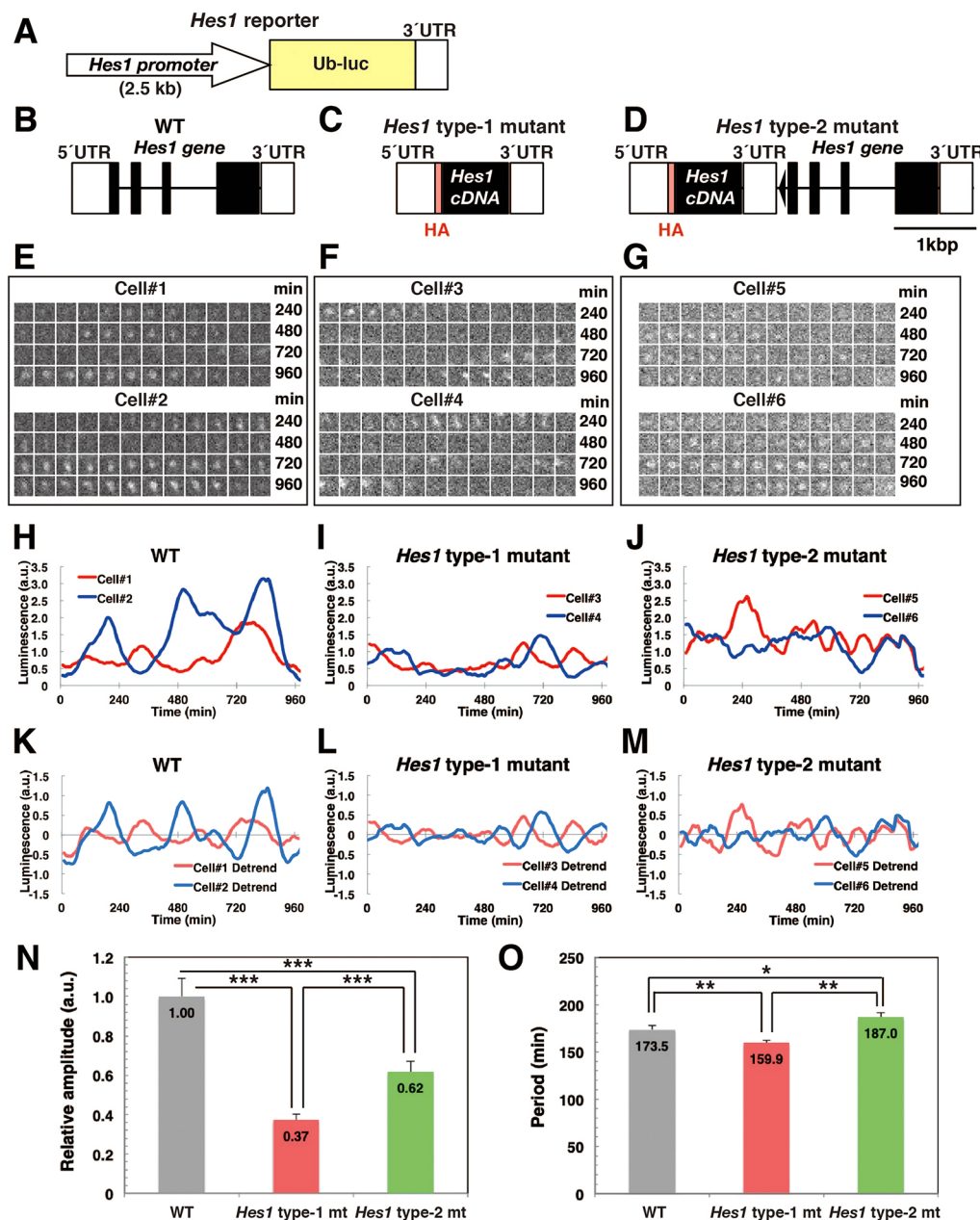
**Fig. 2. *Hes1* expression dynamics in *Hes1* type-1 and type-2 mutant mice.** (A) Structure of the *Hes1* reporter. Ubiquitylated luciferase (Ub-luc) cDNA was placed under the control of 2.5-kb of the *Hes1* promoter. (B-D) Mice carrying the *Hes1* reporter were crossed with wild-type (B), *Hes1* type-1 mutant (C) and *Hes1* type-2 mutant (D) mice. (E-G) Luciferase activities were monitored in NPCs of the crosses described in B-D, respectively. (H-J) Quantification of the luciferase activities monitored as shown in E-G. (K-M) Detrended signals of the luciferase activities monitored in (E-G). (N,O) Average with s.e.m. of the amplitude (N) and period (O) of *Hes1* oscillations. At least 100 cells were examined for each genotype. *$P<0.05$, **$P<0.01$, ***$P<0.001$ (Student's $t$-test). a.u., arbitrary units; WT, wild type.

The brains of *Hes1* type-1 mutant mice were also smaller than those of the wild type at E12.5 and E16.5 (Fig. 4A,C). Immunohistological and *in situ* hybridization analyses showed that the proportions of the nestin[+] and Pax6^{+} cells in the ventricular zone, Tbr2 (Eomes)[+] intermediate progenitor cells, and Tuj1 (Tubb3)[+] neurons were not significantly different between *Hes1* type-1 homozygous mutant and wild-type embryos (Fig. 4D-I). Although expression of the proneural gene *Neurog2* was not significantly different, the proneural gene *Ascl1* was slightly upregulated in *Hes1* type-1 homozygous mutant embryos compared with the wild type at E12.5 (Fig. 4J-L). There were no significant differences in the proportions of Cux1^{+} cells in cortical layers 2-4, Ctip2 (Bcl11b)[+] cells in layer 5, or Tbr1^{+} cells in layer 6 between *Hes1* type-1 homozygous mutant and wild-type embryos (Fig. 4M-O). Furthermore, differentiation of inhibitory neurons [GAD65 (GAD2)[+], GABA[+]] was not affected in the lateral and medial ganglionic eminence (Fig. 4P,Q). We also compared the proliferation and neuronal differentiation of NPC cultures prepared

from E12.5 wild-type and *Hes1* type-1 homozygous mutant embryos but did not find any significant differences (Fig. S6). Together, these results indicated that despite a smaller brain size and upregulation of *Ascl1*, neural development proceeds almost normally in *Hes1* type-1 homozygous mutant embryos.

We next examined whether cell proliferation and death are affected in *Hes1* type-1 homozygous mutant embryos. The number of phospho-histone H3 (pH3)-positive mitotic cells in the apical (ventricular) but not basal region of the *Hes1* type-1 homozygous mutant brain was slightly lower than in the wild type at E12.5, suggesting that proliferation of NPCs decreased in the mutants (Fig. 5A-D). Furthermore, the number of cleaved caspase3^{+} apoptotic cells was slightly higher in the cortical layers (Fig. 5A,E) but not significantly different in the ganglionic eminence (Fig. 5F) of *Hes1* type-1 homozygous mutant brain at E14.5 compared with the wild type. These results suggested that decreased cell proliferation and increased apoptosis led to the smaller brains of *Hes1* type-1 homozygous mutant embryos.
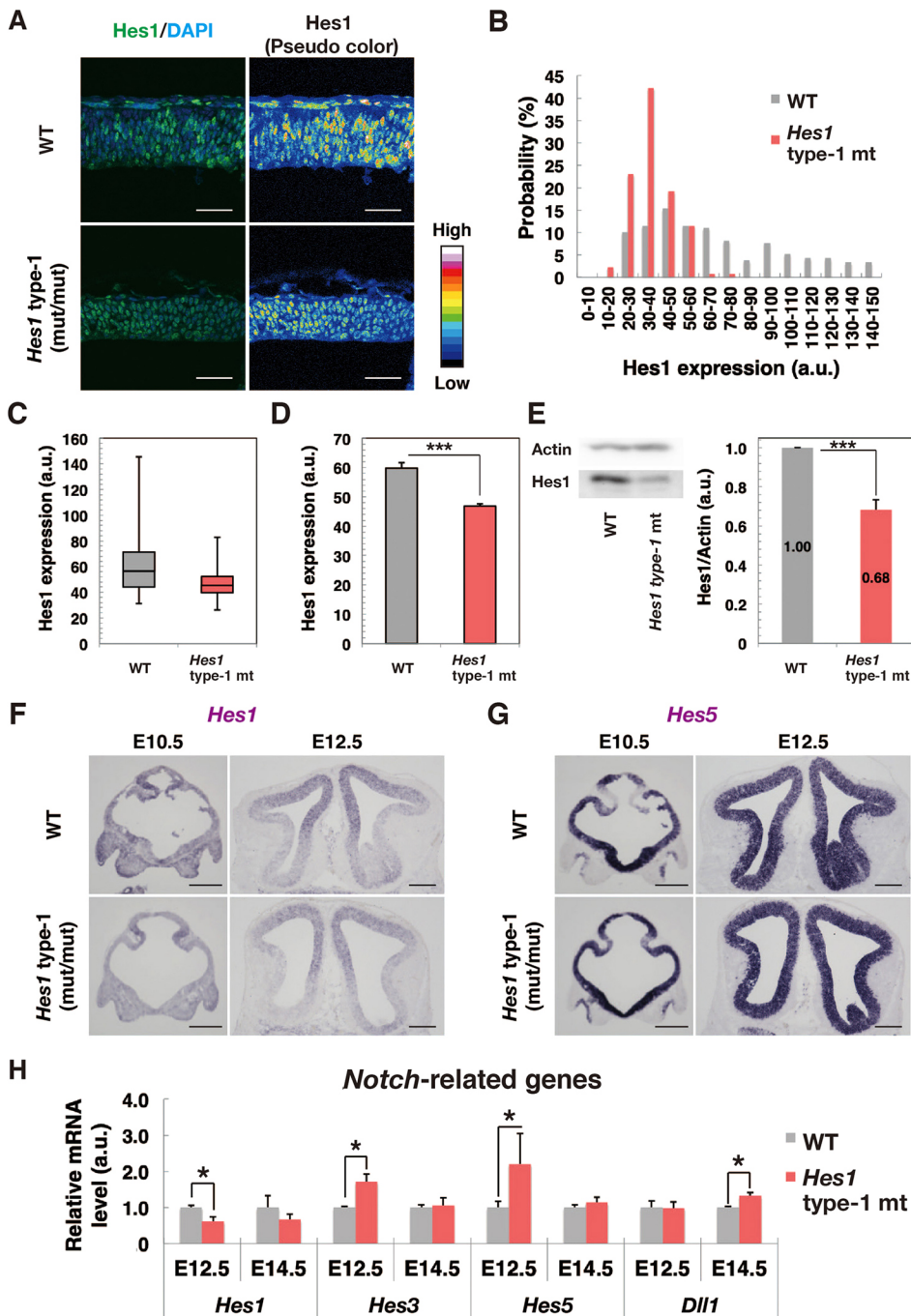
Fig. 3. Hes1 and Hes1-related gene expression in *Hes1* type-1 mutant mice.
(A) Immunohistochemistry of Hes1 in the telencephalon of E10.5 wild-type (WT; top) and *Hes1* type-1 mutant mice (bottom).
(B) Distribution of Hes1 expression levels in NPCs of WT and *Hes1* type-1 mutant mice at E10.5. (C) Box plots of Hes1 expression levels in NPCs at E10.5. In the box plot, the central rectangle ranges from the first quartile to the third quartile, and the middle line represents the median. The whiskers indicate the maximum and minimum. (D) Average levels with s.e.m. of Hes1 expression in WT and *Hes1* type-1 mutant at E10.5. (E) Western blot analysis of Hes1 protein expression in WT and *Hes1* type-1 mutant NPCs. $n=3$ for each genotype. In D and E, ***$P<0.001$ (Student's *t*-test). (F,G) *In situ* hybridization of *Hes1* (F) and *Hes5* (G) in WT (top) and *Hes1* type-1 mutant (bottom) telencephalon. (H) Real-time RT-PCR analyses of gene expression in WT and *Hes1* type-1 mutant mice. Values relative to WT are shown with s.e.m. $n=3$ for each genotype. *$P<0.05$ (Student's *t*-test). Scale bars: 50 μm (A); 300 μm (F,G). a.u., arbitrary units.

In *Hes1* type-1 homozygous mutant mice, both Hes1 protein and *Hes1* mRNA levels were lower at E10.5-E12.5 (Fig. 3D,E,H), and therefore the defects observed in these mutant mice might be due to lower levels of Hes1 expression. To test this possibility, we also examined *Hes1*^{+/−} mice, which had ~60% and ~30% lower levels of *Hes1* mRNA (Fig. S7C) and Hes1 protein (Fig. S7F), respectively. These mice expressed a lower level of *Hes1* mRNA and a similar level of Hes1 protein compared with *Hes1* type-1 homozygous mutant mice (see Fig. 3D,E,H). The analysis of *Hes1* expression dynamics monitored with pHes1-Ub-luc revealed a similar period but a significant reduction in the amplitude of *Hes1* oscillations (Fig. S7A-C,E). However, this reduction in the amplitude is proportional to the reduction in the mean expression value, and the ratio of the amplitude to the mean of *Hes1* oscillations in *Hes1*^{+/−}

NPCs was similar to that in *Hes1* type-2 homozygous mutant but higher than in *Hes1* type-1 homozygous mutant NPCs (Fig. S7D). In *Hes1*^{+/−} mice, we did not find any significant defects in body and brain sizes, proliferation of NPCs, apoptosis, or neuronal differentiation (Fig. S8A,B,E). These results suggest that the defects observed in *Hes1* type-1 homozygous mutant mice were due to dampened *Hes1* oscillations rather than to lower levels of *Hes1* expression.

## Defects of neural development in *Hes1* type-1-mutant;*Hes5*-null embryos

The defects observed in the *Hes1* type-1 homozygous mutant brains were mild, suggesting that *Hes1*-related genes such as *Hes5*, levels of which are also fluctuating (Imayoshi et al., 2013; Manning et al., 2019), may compensate for the *Hes1* abnormality. Therefore, we next
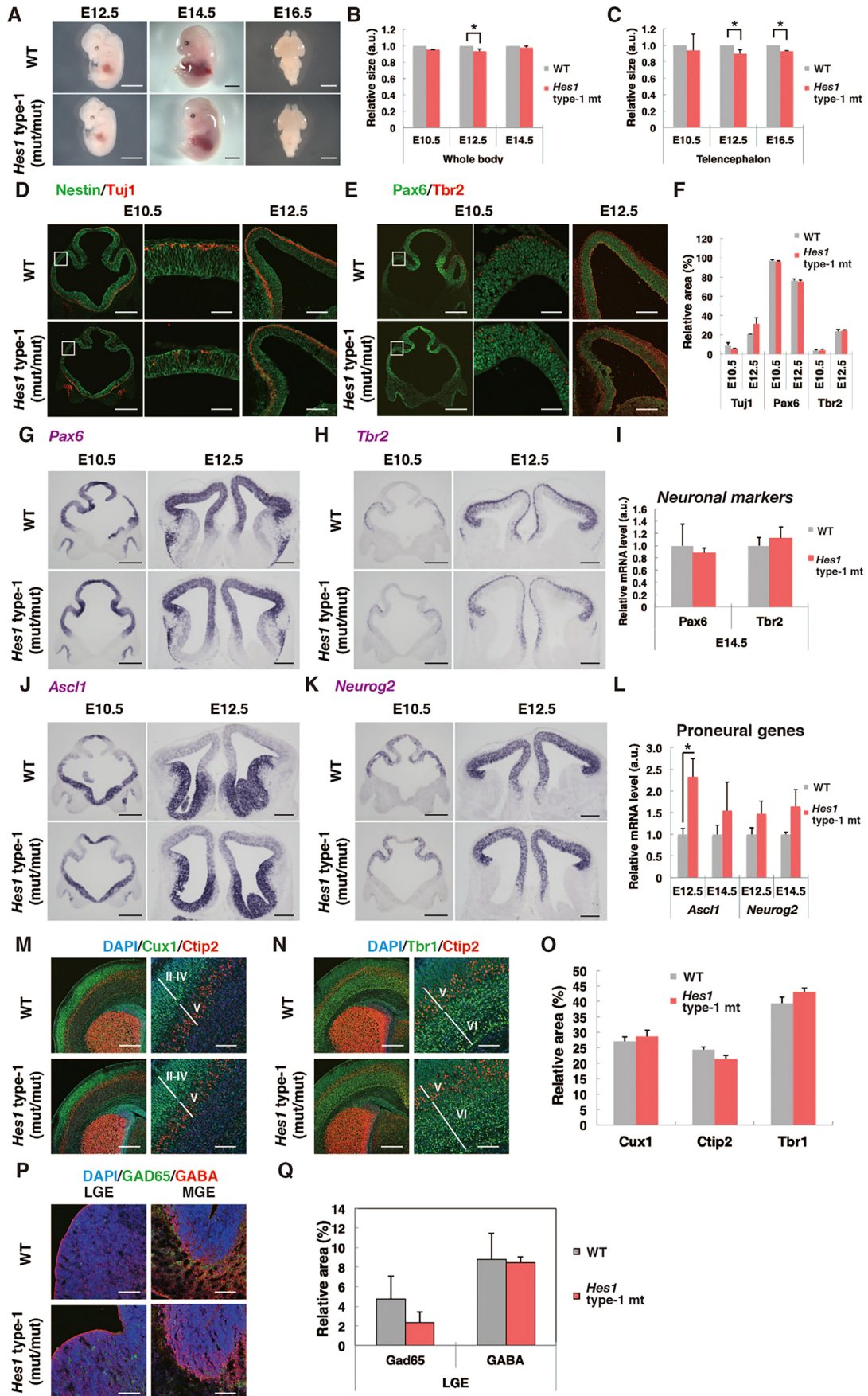
Fig. 4. See next page for legend.

**Fig. 4. Analyses of neural development in *Hes1* type-1 mutant mice.**
(A) Images of the whole body at E12.5 and E14.5 and the telencephalon at
E16.5 of wild-type (WT) and *Hes1* type-1 mutant mice. (B,C) Quantification of
the size (with s.e.m.) of whole body (B) and the telencephalon (C) of WT and
*Hes1* type-1 mutant mouse embryos. For WT, *n*=4 (E10.5), 10 (E12.5), 7
(E14.5) and 4 (E16.5). For *Hes1* type-1 mutant, *n*=3 (E10.5), 10 (E12.5), 7
(E14.5) and 4 (E16.5). (D,E) Immunohistochemistry of nestin, Tuj1, Pax6 and
Tbr2 in the cortex of WT and *Hes1* type-1 mutant mice at E10.5 and E12.5. For
E10.5 images, boxed areas are shown at higher magnification to the right.
(F) Quantification of the thickness (with s.e.m.) of Tuj1$^+$, Pax6$^+$ and Tbr2$^+$
regions in the cortex of WT and *Hes1* type-1 mutant mice. (G,H,J,K) *In situ*
hybridization of *Pax6* (G), *Tbr2* (H), *Ascl1* (J) and *Neurog2* (K) in the
telencephalon of WT and *Hes1* type-1 mutant mice at E10.5 and E12.5.
(I,L) Real-time RT-PCR analyses of *Pax6* (I), *Tbr2* (I), *Ascl1* (L) and *Neurog2*
(L) mRNA expression levels (with s.e.m.) in NPCs in the telencephalon of WT
and *Hes1* type-1 mutant mice at E12.5 and E14.5. (M,N)
Immunohistochemistry of Cux1, Ctip2 and Tbr1 in the cortex of WT and *Hes1*
type-1 mutant mice at P0. (O) Quantification of the thickness (with s.e.m.) of
Cux1$^+$, Ctip2$^+$ and Tbr1$^+$ regions in the cortex of WT and *Hes1* type-1 mutant
mice at P0. Percentages relative to the whole cortical area are shown.
(P) Immunohistochemistry of GAD65 and GABA in the lateral (LGE) and
medial ganglionic eminence (MGE). (Q) Quantification of the area (with s.e.m.)
of GAD65$^+$ and GABA$^+$ regions in the LGE of WT and *Hes1* type-1 mutant mice
at E14.5. Percentages relative to the whole LGE area are shown. At least three
samples were examined for quantification. *$P<0.05$ (Student's *t*-test); a.u.,
arbitrary units. Scale bars: 3 mm (A); 400 µm (D left, E left, M left, N left);
300 µm (G,H,J,K); 200 µm (D right, E right); 100 µm (M right, N right, P); 50 µm
(D middle, E middle).

examined *Hes1* type-1-mutant;*Hes5*-null embryos. Although neural
development is slightly delayed in *Hes5*-null embryos compared with
the wild type (Bansod et al., 2017), the size and the final
morphologies of *Hes5*-null mice are normal (Ohtsuka et al., 1999);
therefore, we used *Hes5*-null mice as controls. The brains of *Hes1*
type-1-mutant;*Hes5*-null embryos were significantly smaller than
those of *Hes5*-null embryos at E12.5 (Fig. 6A,B). They also tended to
be smaller than *Hes5*-null embryos at later stages but this was not
statistically significant (Fig. 6A,B). Immunochemical analyses
showed that there were more Tuj1$^+$ neurons at E14.5 (Fig. 6C,D),
and the number of Tbr2$^+$ intermediate progenitors increased at E12.5
in *Hes1* type-1-mutant;*Hes5*-null embryos, compared with *Hes5*-null
embryos (Fig. 6E,F). Furthermore, there were more Ctip2$^+$ layer 5
neurons at E14.5 in *Hes1* type-1-mutant;*Hes5*-null embryos
compared with *Hes5*-null embryos (Fig. 6G,H), although at
postnatal day (P) 0 Ctip2 expression was not significantly different
(Fig. 6I,J). In addition, there were more Cux1$^+$ layers 2-4 neurons in
*Hes1* type-1-mutant;*Hes5*-null embryos than in *Hes5*-null embryos at
P0 (Fig. 6I,J). Together, these results suggested that neurogenesis was
accelerated in *Hes1* type-1-mutant;*Hes5*-null embryos compared
with *Hes5*-null embryos.

We also examined *Hes1*$^{+/-}$;*Hes5*$^{-/-}$ mice. There were no
significant differences in body and brain sizes (Fig. S8C,D),
neuronal differentiation (Fig. S8F-I), proliferation (Fig. S8J-M) or
apoptosis (Fig. S8J,N) between *Hes1*$^{+/-}$;*Hes5*$^{-/-}$ and *Hes5*$^{-/-}$
mice, suggesting that neural development proceeds almost normally
in *Hes1*$^{+/-}$;*Hes5*$^{-/-}$ mice, and that the defects observed in *Hes1*
type-1-mutant;*Hes5*-null embryos are due to dampened Hes1
oscillations and not to decreased Hes1 expression levels.

### Defects of neural development in *Hes1* type-1-mutant;*Hes3;* *Hes5*-double-null embryos
Because the defects observed in *Hes1* type-1-mutant;*Hes5*-null
embryos could be still compensated by *Hes3*, we next examined the
*Hes1* type-1 mutant in the *Hes3*$^{-/-}$;*Hes5*$^{-/-}$ background. We
previously showed that *Hes3*$^{-/-}$;*Hes5*$^{-/-}$ mice were mostly normal

(Hatakeyama et al., 2004) and therefore used them as controls. The
size of the telencephalon was significantly smaller in *Hes1* type-1-
mutant;*Hes3;Hes5*-double-null embryos than in the controls at
E12.5 (Fig. 7A-D). Furthermore, neurogenesis was increased in the
ventral telencephalon of *Hes1* type-1-mutant;*Hes3;Hes5*-double-
null embryos compared with the controls (Fig. 7C,E), but apoptosis
was not significantly affected (Fig. 7F,G). Thus, *Hes1* type-1
mutation led to microcephaly in the *Hes3*$^{-/-}$;*Hes5*$^{-/-}$ background,
indicating that robust Hes1 oscillations are required for maintenance
and proliferation of NPCs and the normal brain morphogenesis.

## DISCUSSION
### Requirement of robust *Hes1* oscillations for efficient proliferation of NPCs
In this study, to examine the significance of *Hes1* oscillations in
NPCs, we made two types of *Hes1*-mutant mice that altered Hes1
expression dynamics. In *Hes1* type-1 homozygous mutant embryos,
Hes1 oscillations were dampened, and the maintenance and
proliferation of NPCs were reduced. The average levels of Hes1
expression in these mutant NPCs were about 60-70% of those in
wild-type NPCs but slightly higher than (mRNA level) or similar to
(protein level) those in *Hes1* heterozygous mutant mice, which
exhibit no apparent defects. Together, these findings suggest that the
defects observed in *Hes1* type-1 mutant mice are due to dampened
Hes1 oscillations rather than to decreased levels of Hes1. It was
previously shown that Hes1 oscillations periodically repress the
expression of the proneural gene *Ascl1*, driving Ascl1 oscillations,
and that optogenetically induced Ascl1 oscillations promote
proliferation of NPCs (Imayoshi et al., 2013). Furthermore, it was
shown that sustained, high levels of Hes1, which suppress Ascl1
expression, promote quiescence in NPCs (Sueda et al., 2019). These
results indicated that robust Hes1 oscillations and the resultant
proneural gene oscillations are important for efficient proliferation
of NPCs. The defects in *Hes1* type-1 homozygous mutant embryos
were mild, because *Hes1*-related genes, such as *Hes3* and *Hes5*,
compensate for the *Hes1* abnormality. Indeed, when *Hes3* and *Hes5*
were additionally deleted, neurogenesis was enhanced in *Hes1* type-
1 homozygous mutant embryos. These findings suggest that
dampened Hes1 oscillations affect proneural gene oscillations,
which may affect the proliferation and differentiation of NPCs.

In *Hes1* type-2 homozygous mutant mice, Hes1 oscillations were
dampened but less altered than in *Hes1* type-1 homozygous mutant
mice, and *Hes1* type-2 homozygous mutant mice were mostly
normal. Thus, developmental processes may be somewhat resistant
to dampened Hes1 oscillations. This is partly due to compensation
by *Hes1*-related genes such as *Hes3* and *Hes5,* and it remains to be
analyzed whether *Hes1* type-2 homozygous mutant embryos
exhibit any abnormality in the *Hes3*- and/or *Hes5*-null background.

### Deleting introns leads to dampened *Hes1* oscillations
According to mathematical modeling, negative feedback with a
delayed timing is required for oscillatory expression, and negative
feedback at shorter than optimal delays dampens the oscillations
(Fig. S1; Takashima et al., 2011). It has been shown that such delays
depend on intronic delays, the time required for transcription and
splicing of intronic sequences (Swinburne et al., 2008; Swinburne
and Silver, 2008). Indeed, it was previously shown that deletion of
all three introns from the *Hes7* gene accelerates the timing of
negative feedback (faster *Hes7* mRNA/protein formation), leading
to steady (non-oscillatory) *Hes7* expression and severe somite
fusion (Takashima et al., 2011). In *Hes1* type-1 homozygous mutant
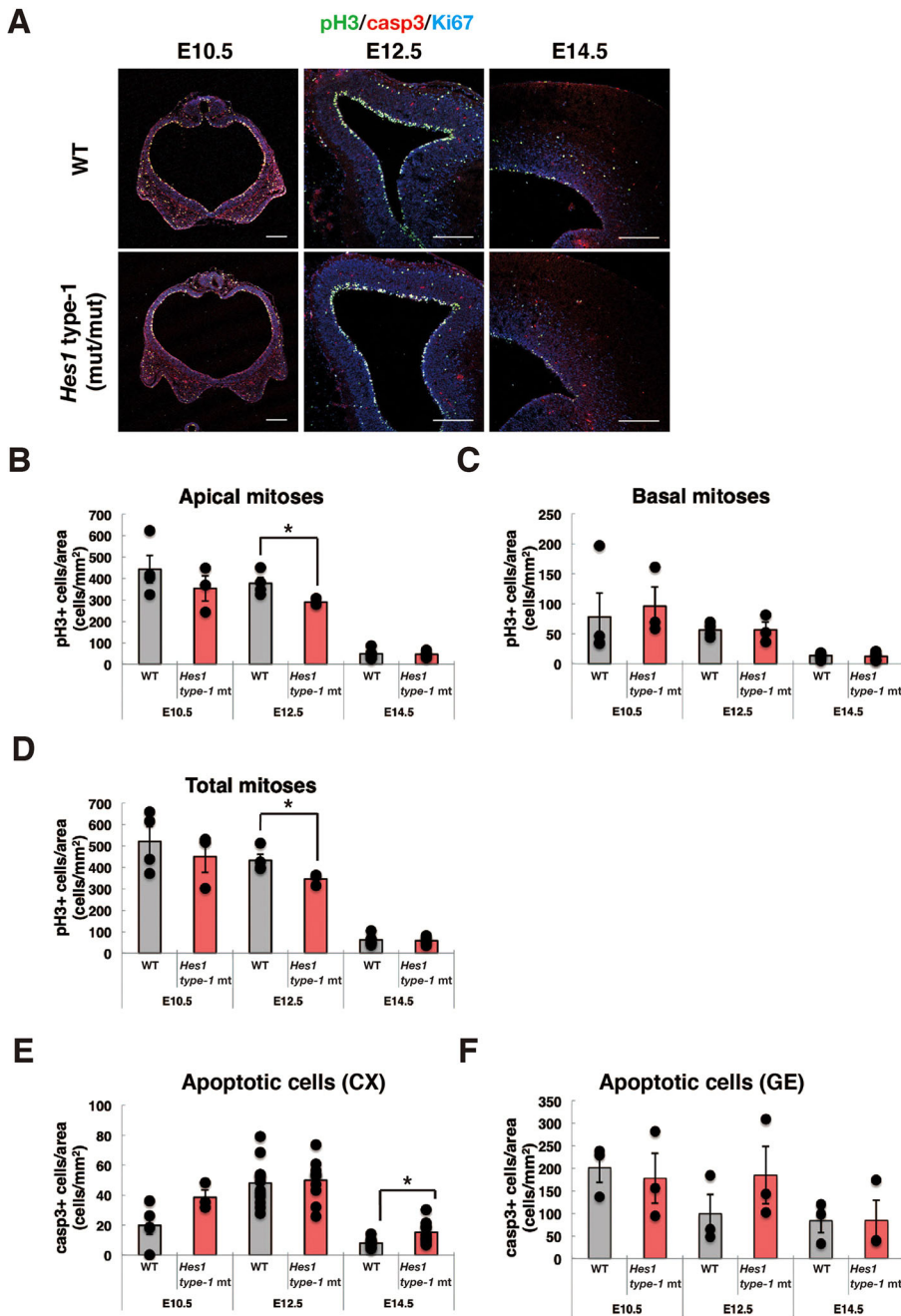embryos, deletion of all three introns led to dampened *Hes1*

7

**Fig. 5. Analyses of cell proliferation and cell death in *Hes1* type-1 mutant mice.**
(A) Immunohistochemistry of phospho-histone H3 (pH3), cleaved caspase3 (casp3) and Ki67 in the cortex of WT and *Hes1* type-1 mutant mice at E10.5, E12.5 and E14.5. Scale bars: 200 μm. (B-F) Quantification of apical mitotic cells (B), basal mitotic cells (C), total number of mitotic cells (D), and apoptotic cells in the cortex (E) and the ganglionic eminence (F) of wild-type and *Hes1* type-1 mutant mice at E10.5, E12.5 and E14.5. Average values with s.e.m. are shown. *$P<0.05$ (Student's *t*-test). At least three samples were examined for each condition.

oscillations, but *Hes1* expression still oscillated unstably with shorter periodicity and smaller amplitudes. In the developing nervous system, gene expression oscillates out of phase with that of neighboring cells (Shimojo et al., 2016), and it has been mathematically suggested that whereas in-phase oscillations observed in the presomitic mesoderm are robust and stable, out-of-phase oscillations are unstable (Yoshioka-Kobayashi et al., 2020). Thus, unstable *Hes1* oscillations in NPCs may be susceptible to interfering noises, and in *Hes1* type-1 homozygous mutant embryos noise produced by cell movements and/or cell division may still induce fluctuations in *Hes1* expression. Another issue is that *Hes1* expression decreased in *Hes1* type-1 mutant NPCs. This decrease could be partly because introns are important for both efficient transport and translation of mRNA. Further analyses are required to understand how the dynamics of in-phase and out-of-phase oscillations are controlled.

As mathematically modeled, the *Hes1* type-2 mutation delays the timing of negative feedback (slower *Hes1* mRNA formation) and leads to *Hes1* oscillations with longer periodicity. However, although modeling suggests that slower negative feedback generates oscillations with higher amplitudes, the actual amplitudes of *Hes1* oscillations in *Hes1* type-2 homozygous mutant embryos were smaller than those in wild-type embryos. This might be partly due to nonsense-mediated mRNA decay (He and Jacobson, 2015), which is often observed when the stop codon is present in the first exon, but the exact mechanism remains to be analyzed.

## The mechanism by which Hes1 and proneural gene oscillations regulate cell proliferation and differentiation
Our data suggest that robust Hes1 and proneural gene oscillations are necessary for efficient proliferation of NPCs. This notion agrees well with previous data demonstrating that dampened *Hes1*
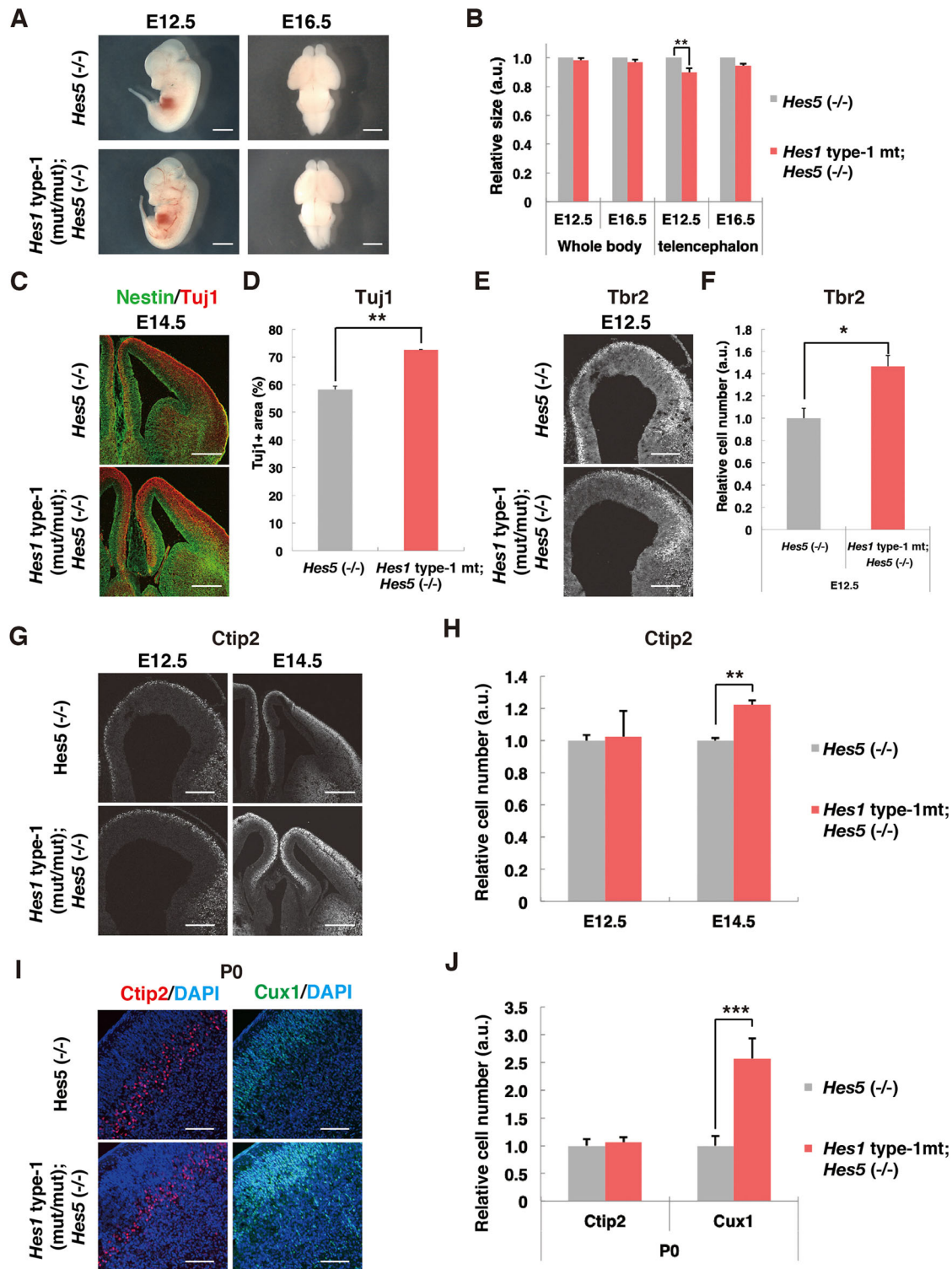
**Fig. 6. Analyses of neurogenesis in *Hes1* type-1-mutant;*Hes5*-null mice.** (A) Images of the whole body at E12.5 and the brain at E16.5 of *Hes5*-null and *Hes1* type-1-mutant;*Hes5*-null mice. (B) Quantification of the whole body and telencephalon sizes (with s.e.m.) of *Hes5*-null mice and *Hes1* type-1-mutant; *Hes5*-null mice. For *Hes5*$^{-/-}$, $n$=6 (E12.5) and 6 (E16.5). For *Hes1* type-1 mutant;*Hes5*$^{-/-}$, $n$=7 (E12.5) and 7 (E16.5). (C,E,G,I) Immunohistochemistry of nestin (C), Tuj1 (C), Tbr2 (E), Ctip2 (G,I) and Cux1 (I) in the cortex of *Hes5*-null and *Hes1* type-1-mutant;*Hes5*-null mice. (D,F,H,J) Quantification of the proportions (with s.e.m.) of Tuj1$^+$ (D), Tbr2$^+$ (F), Ctip2$^+$ (H,J) and Cux1$^+$ (J) cell formation in the cortex of *Hes5*-null mice and *Hes1* type-1-mutant;*Hes5*-null mice. At least three samples were examined for quantification. *$P$<0.05, **$P$<0.01, ***$P$<0.001 (Student's $t$-test). Scale bars: 2 mm (A); 400 μm (C); 200 μm (E,G); 100 μm (I).

oscillations induced by accelerated or delayed Dll1 expression resulted in inhibition of NPC proliferation and acceleration of neurogenesis (Shimojo et al., 2016). Similarly, it was recently

shown that Hes1 oscillations drive oscillatory expression of the muscle determination factor MyoD in activated muscle progenitors, and that Hes1 and MyoD oscillations may be important for
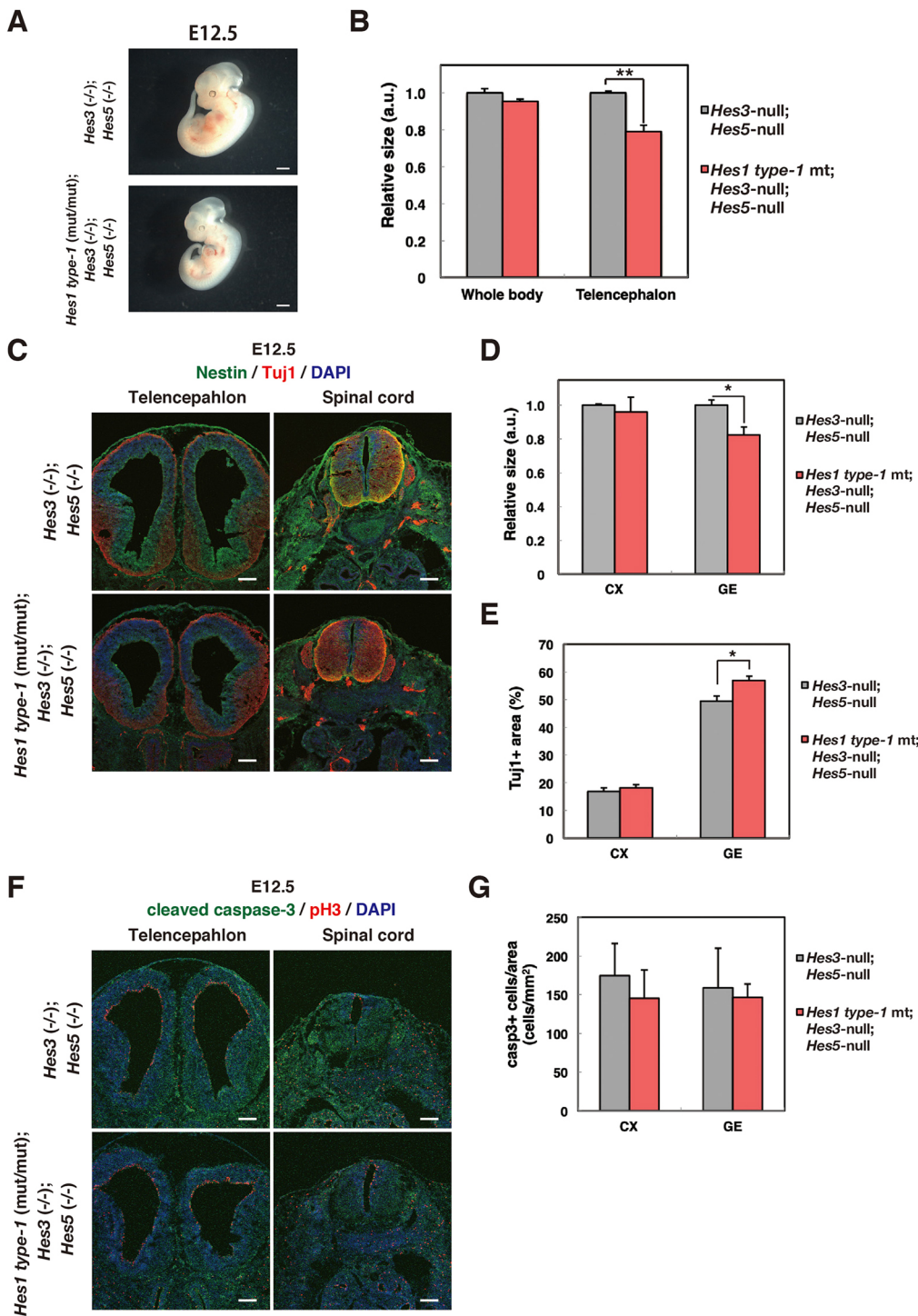
DEVELOPMENT

9

**Fig. 7. Analyses of neurogenesis in Hes1 type-1-mutant;Hes3$^{-/-}$;Hes5$^{-/-}$ mice.** (A) Images of the whole body at E12.5 of Hes3$^{-/-}$;Hes5$^{-/-}$ and Hes1 type-1-mutant;Hes3$^{-/-}$;Hes5$^{-/-}$ mice. (B,D) Size quantification (with s.e.m.) of the whole body (B), telencephalon (B), cortex (CX; D) and ganglionic eminence (GE; D) of Hes3$^{-/-}$;Hes5$^{-/-}$ and Hes1 type-1-mutant;Hes3$^{-/-}$; Hes5$^{-/-}$ mice at E12.5. (C,F) Immunohistochemistry of nestin (C), Tuj1 (C), cleaved caspase3 (F) and phospho-histone H3 (pH3) (F) in the telencephalon and spinal cord of Hes3$^{-/-}$;Hes5$^{-/-}$ and Hes1 type-1-mutant;Hes3$^{-/-}$;Hes5$^{-/-}$ mice at E12.5. (E,G) Quantification of the area (with s.e.m.) of Tuj1 staining (E) and the number of cells expressing cleaved caspase3 (G) in the CX and GE of Hes3$^{-/-}$;Hes5$^{-/-}$ and Hes1 type-1-mutant;Hes3$^{-/-}$;Hes5$^{-/-}$ mice at E12.5. n=3 for each genotype. *P<0.05, **P<0.01 (Student's t-test). Scale bars: 2 mm (A); 400 µm (C,F).

proliferation and differentiation of muscle progenitors (Lahmann et al., 2019). Furthermore, it has been shown that high and sustained levels of Hes1 repress the expression of cell cycle regulators and lead to G1 arrest in cultured fibroblasts, NPCs and hematopoietic stem cells (Baek et al. 2006; Yu et al., 2006; Sang et al., 2008), suggesting that high and sustained Hes1 is a general feature of maintaining quiescence in many cell types. However, the exact mechanism by which oscillations activate cell proliferation remains to be analyzed. Genes upregulated by oscillatory and downregulated by sustained levels of Hes1, or vice versa, should be determined to understand whether genes, particularly those involved in cell cycle progression, are differentially controlled by the two modes of Hes1 expression.

Another important issue is how the timing of neuronal differentiation is regulated. When Hes1 oscillations were dampened in Hes1 type-1-mutant;Hes5-null and Hes1 type-1-mutant;Hes3; Hes5-double-null embryos, neurogenesis was enhanced compared with the controls, suggesting that Hes1 oscillations play an important role in the normal timing of neurogenesis. Dampened Hes1 oscillations may also dampen proneural gene oscillations, and

sustained proneural gene expression might lead to enhanced neurogenesis. It was previously shown that Dll1 oscillations, which are controlled by Hes1 and proneural gene oscillations, are important for the normal timing of neurogenesis (Shimojo et al., 2016). In *Hes1* type-1 mutant embryos, Dll1 oscillations might be dampened by dampened Hes1 and proneural gene oscillations, and sustained Dll1 expression may affect the timing of neurogenesis, because sustained Dll1 overexpression induces neuronal differentiation in a non-cell-autonomous manner (Kawaguchi et al., 2008). Taken together, our results suggest that robust *Hes1* oscillations play an important role in efficient proliferation and maintenance of NPCs and normal brain morphogenesis.

## MATERIALS AND METHODS

### Animals and generation of *Hes1* type-1 and type-2 mutant mice

All animal experiments were approved by the Institutional Animal Care and Use Committee at Kyoto University. *Hes3*- and *Hes5*-null mice and Hes1 reporter mice were previously described (Hatakeyama et al., 2004; Shimojo et al., 2008).

For generation of *Hes1* type-1 mutant mice, the *Hes1* gene from ATG to the stop codon were replaced with HA sequence-fused *Hes1* cDNA by BAC recombineering. In the case of *Hes1* type-2 mutant mice, HA sequence-fused *Hes1* cDNA followed by the 3′UTR of the *Hes1* gene were inserted between the 5′UTR and the initiation codon of *Hes1* by BAC recombineering. For preparation of the targeting vector of the *Hes1* type-1 mutant, an FRT-Neo[R] cassette was inserted into the downstream region of the 3′UTR. The region from 2.5 kb upstream of the HA sequence to 8.0 kb downstream of the FRT-Neo[R] cassette was retrieved to the pMCS-DTA vector. For preparation of the targeting vector of the *Hes1* type-2 mutant, an FRT-Neo[R] cassette was inserted into the downstream region of the 3′UTR following the *Hes1* cDNA sequence, and the region from 1.7 kb upstream of the HA sequence to 6.0 kb downstream of the FRT-Neo[R] cassette was retrieved to the pMCS-DTA vector. The linearized targeting vectors were electroporated into TT2 ESCs, and G418-resistant clones were screened by PCR. The homologous recombinant ESC clones were injected into eight-cell stage mouse embryos to obtain chimeric mice. Chimeric mice were crossed with pCAG-FLP mice to delete the Neo sequence.

### Bioluminescence imaging of NPC dissociation culture

*Hes1* type-1 and type-2 mutant mice were crossed with Hes1 reporter mice. NPCs were prepared from the cortex of E12.5 and E14.5 wild-type embryos and *Hes1* type-1 and type-2 mutant embryos that carried the Hes1 reporter. The protocol of dissociation culture using the Papain Dissociation System (Worthington) was described previously (Shimojo et al., 2008, 2016). Dissociated NPCs (2.0-3.0×10^6 cells/ml) were plated into ϕ12-mm or ϕ27-mm glass-bottom dishes (IWAKI) with 1 mM luciferin (Nacalai Tesque) in N2/B27 medium [DMEM/F12 supplemented with 1× N2 (Thermo Fisher Scientific), 1× B27 (Thermo Fisher Scientific), 1 mM N-acetyl-cysteine, 10 ng/ml bFGF (Thermo Fisher Scientific)]. After a 1-h pre-incubation, cells were cultured in medium containing luciferin for measurement of bioluminescence. The dish was placed on the stage of an inverted microscope (Olympus IX81) and was maintained at 37°C. Bioluminescence was measured using an Olympus objective lens (UPLFLN 40 O) and was transmitted directly to a CCD camera (Princeton Instruments, VersArray 1 kb), as previously described (Shimojo et al., 2008, 2016).

### Image processing and time-series analysis

Images were processed using Fiji image analysis software. Stack images were processed using the Spike Noise Filter to remove signals from cosmic rays and then the Savitzky Golay Temporal Filter to get clear dynamic expression. Period and amplitude of oscillatory expression were measured by single cell tracking (Webb et al., 2016). Detrended fluctuation analysis (DFA) was used for determining self-affinity of a signal, and the time series was detrended by subtracting the moving average within a 240 min window. To calculate moving averages near the edges (initial and late 120 min frames

in the time series), data-padding was performed by mirroring. Extreme values were extracted manually, and periods shorter than 60 min and longer than 250 min were discarded. The amplitude was calculated as the average of peak heights relative to the mean (in arbitrary units).

### Immunostaining

Embryos and brains were dissected and fixed in 4% paraformaldehyde overnight at 4°C. After being washed in PBS, equilibrated in 25% sucrose/PBS overnight at 4°C and then embedded in OCT compound, tissues were sectioned at 16 μm using a cryostat (CM1950, Leica). NPC cultures were fixed in 4% paraformaldehyde for 20 min at room temperature. For immunostaining of Hes1, antigen retrieval was performed in 0.1% Tween20/0.01 M citrate buffer (pH 6.0) using an autoclave (15 min at 105°C). Sections were incubated with primary antibody (rabbit anti-Hes1; Kobayashi et al., 2009) overnight at 4°C. After being washed in PBS, sections were incubated with secondary antibody (HRP-conjugated anti-rabbit IgG) for 90 min at room temperature. After washes in PBS and PBST (PBS with 0.3% Triton X-100), color development was enhanced using the TSA amplification system (Perkin Elmer) according to the manufacturer's instructions. For immunostaining of Pax6, Tbr2, Tbr1 and Cux1, antigen retrieval was performed in 0.1% Tween20/0.01 M citrate buffer (pH 6.0) using an autoclave (15 min at 105°C). Primary antibodies used were as follows: mouse anti-Pax6, rabbit anti-Tbr2, rabbit anti-Tbr1, rabbit anti-Cux1, mouse anti-nestin, rabbit anti-Tuj1, mouse anti-pH3, rabbit anti-cleaved-casp3, mouse anti-GAD65 and rabbit anti-GABA. Sections were incubated with primary antibodies overnight at 4°C. The secondary antibodies used were as follows: Alexa 488-conjugated anti-mouse IgG, Alexa 594-conjugated anti-rabbit IgG, Alexa 488-conjugated anti-rabbit IgG and Alexa 594-conjugated anti-rat IgG. Antibody details are listed in Table S1.

### *In situ* hybridization

Preparation of DIG-labeled antisense RNA probes and *in situ* hybridization using NBT/BCIP (Roche) detection were performed as described previously (Bessho et al., 2001; Shimojo et al., 2008).

### PCR analysis

Samples were collected from the telencephalon of each embryo, total RNA was extracted, and then reverse transcription (RT) reaction was performed. Real-time PCR (qPCR) was performed as described previously (Kobayashi et al., 2009). Quantified values of RNA were normalized with those of *Gapdh*. Primers are listed in Table S2. At least three embryos of each genotype were examined.

### Analysis of the distribution of Hes1 protein expression

The intensity of Hes1 immunostaining of individual NPCs in the cortex of each genotype was measured using Fiji software, as previously described (Baek et al., 2006).

### Western blot analysis

Western blot analysis of Hes1 was performed as previously described (Hirata et al., 2002).

### Measurements of the size of the whole body and the telencephalon

Images of embryos were obtained using a stereomicroscope (MZ16 FA, Leica). The length of the long axis and the area of the whole body and of the telencephalon were measured using Fiji software. Quantified values of mutants were compared with those of control mice. At least three embryos of each genotype were examined.

### Measurement of the formation of neuronal layers

The area or the number of cells expressing each neuronal marker (Tuj1, Tbr2, Cux1, Ctip2, Tbr1) in the cortex of each embryo was measured using Fiji software. For the quantification of neuronal layers, serial 16-μm sections were cut, and every 20th section was used. At least three embryos of each genotype were examined.

## Measurement of the number of mitotic and apoptotic cells

pH3$^+$ mitotic cells in the cortex were classified into apical or basal mitoses (Cárdenas et al., 2018). The numbers of pH3$^+$ mitotic and cleaved caspase3$^+$ apoptotic cells were counted. At least three embryos of each genotype were examined.

## NPC and neurosphere cultures

NPC and neurosphere cultures were performed, as previously described (Ohtsuka et al., 2006; Imayoshi et al., 2013). For cell cycle exit analysis, 10 μM 5-bromo-2′-deoxyuridine (BrdU) was added to NPCs, which were then fixed 24 h later and subjected to immunostaining for BrdU and Ki67 (Mki67). The proportion of BrdU$^+$Ki67$^-$ cell number over BrdU$^+$ cell number was calculated.

## Delay measurement of Hes1 expression

Luc2-fused control, *Hes1* type-1 and *Hes1* type-2 vectors were transfected into C2C12 cells and NSCs. Synchronized Hes1 expression in transfected cells was induced by application of 5% fetal bovine serum (Harima et al., 2013). The kinetics of Hes1 expression in these cells were measured using a photomultiplier tube (CL24B-LIC/B, Churitsu Electric Corporation).

## Mathematical simulation

Hes1 oscillations were simulated with the following equations described previously (Hirata et al., 2004; Takashima et al., 2011; Harima et al., 2013):

$$\frac{dp(t)}{dt} = am(t - T_p) - bp(t)$$
$$\frac{dm(t)}{dt} = f(p(t - T_m)) - cm(t),$$

where $p(t)$ and $m(t)$ are the quantities of functional Hes1 protein and *Hes1* mRNA per cell at time $t$, respectively, and $f(p)$ is the rate of initiation of transcription, which depends on the amount of the protein, $p$, present at the time of initiation. $a$ is the rate constant for translation, and $b$ and $c$ are the degradation rate constants for Hes1 protein and *Hes1* mRNA, respectively, which are simply related to the half-lives of Hes1 protein ($\tau_p$) and *Hes1* mRNA ($\tau_m$):

$$b = \frac{ln2}{\tau_p}, \quad c = \frac{ln2}{\tau_m}.$$

Because transcription is inhibited by Hes1 protein, which acts as a dimer, we assume the following:

$$f(p) = \frac{k}{1 + (p/p_{crit})^2},$$

where $k$ is the number of molecules of *Hes1* mRNA synthesized per unit time in the absence of inhibition and $p_{crit}$ is the amount of protein that gives half-maximal inhibition. We set $a$=4.5 protein molecules per mRNA molecule per min, $p_{crit}$=40 molecules per cell, $k$=33 mRNA molecules per cell per min, and $\tau_m$=3 min. We assume that the Hes1 protein half-life $\tau_p$=20 min, the translational delay $T_p$=8 min, and the transcriptional delay $T_m$=29 min. Under these conditions, oscillatory expression continues. When $T_m$=34 min (5 min longer), oscillations are maintained. In contrast, when $T_m$=10 min (19 min shorter) and $T_m$=15.5 min (13.5 min shorter), oscillations are dampened. The figure of Hes1 dynamics (Fig. S1) was exported from the mathematical model using XPPAUT.

## Competing interests

The authors declare no competing or financial interests.

## Author contributions

Conceptualization: S.O., H.S., R.K.; Methodology: S.O., Y.I., H.S., H.M.; Validation: S.O., Y.I., H.S.; Formal analysis: S.O., Y.I., H.S., H.M., R.K.; Investigation: S.O., Y.I., H.S., R.K.; Resources: S.O., Y.I., H.S., H.M.; Data curation: S.O., Y.I., H.S.; Writing - original draft: S.O., H.S., R.K.; Writing - review & editing: H.S., R.K.; Visualization: H.S.; Supervision: H.S., R.K.; Project administration: R.K.; Funding acquisition: H.S., R.K.

## Supplementary information

Supplementary information available online at
http://dev.biologists.org/lookup/doi/10.1242/dev.182204.supplemental

## References

**Albeck, J. G., Mills, G. B. and Brugge, J. S.** (2013). Frequency-modulated pulses of ERK activity transmit quantitative proliferation signals. *Mol. Cell* **49**, 249-261. doi:10.1016/j.molcel.2012.11.002

**Aoki, K., Kumagai, Y., Sakurai, A., Komatsu, N., Fujita, Y., Shionyu, C. and Matsuda, M.** (2013). Stochastic ERK activation induced by noise and cell-to-cell propagation regulates cell density-dependent proliferation. *Mol. Cell* **52**, 529-540. doi:10.1016/j.molcel.2013.09.015

**Ashall, L., Horton, C. A., Nelson, D. E., Paszek, P., Harper, C. V., Sillitoe, K., Ryan, S., Spiller, D. G., Unitt, J. F., Broomhead, D. S. et al.** (2009). Pulsatile stimulation determines timing and specificity of NF-κB-dependent transcription. *Science* **324**, 242-246. doi:10.1126/science.1164860

**Baek, J. H., Hatakeyama, J., Sakamoto, S., Ohtsuka, T. and Kageyama, R.** (2006). Persistent and high levels of Hes1 expression regulate boundary formation in the developing central nervous system. *Development* **133**, 2467-2476. doi:10.1242/dev.02403

**Bansod, S., Kageyama, R. and Ohtsuka, T.** (2017). Hes5 regulates the transition timing of neurogenesis and gliogenesis in mammalian neocortical development. *Development* **144**, 3156-3167. doi:10.1242/dev.147256

**Bessho, Y., Sakata, R., Komatsu, S., Shiota, K., Yamada, S. and Kageyama, R.** (2001). Dynamic expression and essential functions of *Hes7* in somite segmentation. *Genes Dev.* **15**, 2642-2647. doi:10.1101/gad.930601

**Bessho, Y., Hirata, H., Masamizu, Y. and Kageyama, R.** (2003). Periodic repression by the bHLH factor Hes7 is an essential mechanism for the somite segmentation clock. *Genes Dev.* **17**, 1451-1456. doi:10.1101/gad.1092303

**Bonev, B., Stanley, P. and Papalopulu, N.** (2012). MicroRNA-9 modulates *Hes1* ultradian oscillations by forming a double-negative feedback loop. *Cell Rep.* **2**, 10-18. doi:10.1016/j.celrep.2012.05.017

**Cárdenas, A., Villalba, A., De Juan Romero, C., Picó, E., Kyrousi, C., Tzika, A. C., Tessier-Lavigne, M., Ma, L., Drukker, M., Cappello, S. et al.** (2018). Evolution of cortical neurogenesis in amniotes controlled by Robo signaling levels. *Cell* **174**, 590-606.e21. doi:10.1016/j.cell.2018.06.007

**Castro, D. S., Martynoga, B., Parras, C., Ramesh, V., Pacary, E., Johnston, C., Drechsel, D., Lebel-Potter, M., Garcia, L. G., Hunt, C. et al.** (2011). A novel function of the proneural factor Ascl1 in progenitor proliferation identified by genome-wide characterization of its targets. *Genes Dev.* **25**, 930-945. doi:10.1101/gad.627811

**Chen, F., Zhang, C., Wu, H., Ma, Y., Luo, X., Gong, X., Jiang, F., Gui, Y., Zhang, H. and Lu, F.** (2017). The E3 ubiquitin ligase SCF$^{FBXL14}$ complex stimulates neuronal differentiation by targeting the Notch signaling factor HES1 for proteolysis. *J. Biol. Chem.* **292**, 20100-20112. doi:10.1074/jbc.M117.815001

**Harima, Y., Takashima, Y., Ueda, Y., Ohtsuka, T. and Kageyama, R.** (2013). Accelerating the tempo of the segmentation clock by reducing the number of introns in the *Hes7* gene. *Cell Rep.* **3**, 1-7. doi:10.1016/j.celrep.2012.11.012

**Hatakeyama, J., Bessho, Y., Katoh, K., Ookawara, S., Fujioka, M., Guillemot, F. and Kageyama, R.** (2004). *Hes* genes regulate size, shape and histogenesis of the nervous system by control of the timing of neural stem cell differentiation. *Development* **131**, 5539-5550. doi:10.1242/dev.01436

**He, F. and Jacobson, A.** (2015). Nonsense-mediated mRNA decay: degradation of defective transcripts is only part of the story. *Annu. Rev. Genet.* **49**, 339-366. doi:10.1146/annurev-genet-112414-054639

**Hirata, H., Yoshiura, S., Ohtsuka, T., Bessho, Y., Harada, T., Yoshikawa, K. and Kageyama, R.** (2002). Oscillatory expression of the bHLH factor Hes1 regulated by a negative feedback loop. *Science* **298**, 840-843. doi:10.1126/science.1074560

**Hirata, H., Bessho, Y., Kokubu, H., Masamizu, Y., Yamada, S., Lewis, J. and Kageyama, R.** (2004). Instability of Hes7 protein is crucial for the somite segmentation clock. *Nat. Genet.* **36**, 750-754. doi:10.1038/ng1372

**Hoffmann, A., Levchenko, A., Scott, M. L. and Baltimore, D.** (2002). The IκB−NF-κB signaling module: temporal control and selective gene activation. *Science* **298**, 1241-1245. doi:10.1126/science.1071914

DEVELOPMENT

Imayoshi, I. and Kageyama, R. (2014). bHLH factors in self-renewal, multipotency, and fate choice of neural progenitor cells. *Neuron* 82, 9-23. doi:10.1016/j.neuron. 2014.03.018

Imayoshi, I., Isomura, A., Harima, Y., Kawaguchi, K., Kori, H., Miyachi, H., Fujiwara, T., Ishidate, F. and Kageyama, R. (2013). Oscillatory control of factors determining multipotency and fate in mouse neural progenitors. *Science* 342, 1203-1208. doi:10.1126/science.1242366

Ishibashi, M., Ang, S. L., Shiota, K., Nakanishi, S., Kageyama, R. and Guillemot, F. (1995). Targeted disruption of mammalian *hairy* and *Enhancer of split* homolog-1 (*HES*-1) leads to up-regulation of neural helix-loop-helix factors, premature neurogenesis, and severe neural tube defects. *Genes Dev.* 9, 3136-3148. doi:10. 1101/gad.9.24.3136

Isomura, A. and Kageyama, R. (2014). Ultradian oscillations and pulses: coordinating cellular responses and cell fate decisions. *Development* 141, 3627-3636. doi:10.1242/dev.104497

Johnson, H. E. and Toettcher, J. E. (2019). Signaling dynamics control cell fate in the early Drosophila embryo. *Dev. Cell* 48, 361-370.e3. doi:10.1016/j.devcel. 2019.01.009

Jouve, C., Palmeirim, I., Henrique, D., Beckers, J., Gossler, A., Ish-Horowicz, D. and Pourquié, O. (2000). Notch signalling is required for cyclic expression of the hairy-like gene *HES1* in the presomitic mesoderm. *Development* 127, 1421-1429.

Kawaguchi, D., Yoshimatsu, T., Hozumi, K. and Gotoh, Y. (2008). Selection of differentiating cells by different levels of delta-like 1 among neural precursor cells in the developing mouse telencephalon. *Development* 135, 3849-3858. doi:10. 1242/dev.024570

Kobayashi, T., Mizuno, H., Imayoshi, I., Furusawa, C., Shirahige, K. and Kageyama, R. (2009). The cyclic gene *Hes1* contributes to diverse differentiation responses of embryonic stem cells. *Genes Dev.* 23, 1870-1875. doi:10.1101/gad. 1823109

Lahmann, I., Bröhl, D., Zyrianova, T., Isomura, A., Czajkowski, M. T., Kapoor, V., Griger, J., Ruffault, P.-L., Mademtzoglou, D., Zammit, P. S. et al. (2019). Oscillations of MyoD and Hes1 proteins regulate the maintenance of activated muscle stem cells. *Genes Dev.* 33, 524-534. doi:10.1101/gad.322818.118

Levine, J. H., Lin, Y. and Elowitz, M. B. (2013). Functional roles of pulsing in genetic circuits. *Science* 342, 1193-1200. doi:10.1126/science.1239999

Lewis, J. (2003). Autoinhibition with transcriptional delay: a simple mechanism for the zebrafish somitogenesis oscillator. *Curr. Biol.* 13, 1398-1408. doi:10.1016/ S0960-9822(03)00534-7

Manning, C. S., Biga, V., Boyd, J., Kursawe, J., Ymisson, B., Spiller, D. G., Sanderson, C. M., Galla, T., Rattray, M. and Papalopulu, N. (2019). Quantitative single-cell live imaging links HES5 dynamics with cell-state and fate in murine neurogenesis. *Nat. Commun.* 10, 2835. doi:10.1038/s41467-019-10734-8

Masamizu, Y., Ohtsuka, T., Takashima, Y., Nagahara, H., Takenaka, Y., Yoshikawa, K., Okamura, H. and Kageyama, R. (2006). Real-time imaging of the somite segmentation clock: revelation of unstable oscillators in the individual presomitic mesoderm cells. *Proc. Natl. Acad. Sci. USA* 103, 1313-1318. doi:10. 1073/pnas.0508658103

Monk, N. A. M. (2003). Oscillatory expression of Hes1, p53, and NF-kappaB driven by transcriptional time delays. *Curr. Biol.* 19, 1409-1413. doi:10.1016/S0960-9822(03)00494-9

Nelson, D. E., Ihekwaba, A. E. C., Elliott, M., Johnson, J. R., Gibney, C. A., Foreman, B. E., Nelson, G., See, V., Horton, C. A., Spiller, D. G. et al. (2004). Oscillations in NF-κB signaling control the dynamics of gene expression. *Science* 306, 704-708. doi:10.1126/science.1099962

Oates, A. C., Morelli, L. G. and Ares, S. (2012). Patterning embryos with oscillations: structure, function and dynamics of the vertebrate segmentation clock. *Development* 139, 625-639. doi:10.1242/dev.063735

Ohtsuka, T., Ishibashi, M., Gradwohl, G., Nakanishi, S., Guillemot, F. and Kageyama, R. (1999). *Hes1* and *Hes5* as Notch effectors in mammalian neuronal differentiation. *EMBO J.* 18, 2196-2207. doi:10.1093/emboj/18.8.2196

Ohtsuka, T., Imayoshi, I., Shimojo, H., Nishi, E., Kageyama, R. and McConnell, S. K. (2006). Visualization of embryonic neural stem cells using Hes promoters in transgenic mice. *Mol. Cell. Neurosci.* 31, 109-122. doi:10.1016/j.mcn.2005.09. 006

Pourquié, O. (2011). Vertebrate segmentation: from cyclic gene networks to scoliosis. *Cell* 145, 650-663. doi:10.1016/j.cell.2011.05.011

Purvis, J. E. and Lahav, G. (2013). Encoding and decoding cellular information through signaling dynamics. *Cell* 152, 945-956. doi:10.1016/j.cell.2013.02.005

Sang, L., Coller, H. A. and Roberts, J. M. (2008). Control of the reversibility of cellular quiescence by the transcriptional repressor HES1. *Science* 321, 1095-1100. doi:10.1126/science.1155998

Shimojo, H., Ohtsuka, T. and Kageyama, R. (2008). Oscillations in Notch signaling regulate maintenance of neural progenitors. *Neuron* 58, 52-64. doi:10.1016/j. neuron.2008.02.014

Shimojo, H., Isomura, A., Ohtsuka, T., Kori, H., Miyachi, H. and Kageyama, R. (2016). Oscillatory control of Delta-like1 in cell interactions regulates dynamic gene expression and tissue morphogenesis. *Genes Dev.* 30, 102-116. doi:10. 1101/gad.270785.115

Sueda, R., Imayoshi, I., Harima, Y. and Kageyama, R. (2019). High Hes1 expression and resultant Ascl1 suppression regulate quiescent vs. active neural stem cells in the adult mouse brain. *Genes Dev.* 33, 511-523. doi:10.1101/gad. 323196.118

Swinburne, I. A. and Silver, P. A. (2008). Intron delays and transcriptional timing during development. *Dev. Cell* 14, 324-330. doi:10.1016/j.devcel.2008.02.002

Swinburne, I. A., Miguez, D. G., Landgraf, D. and Silver, P. A. (2008). Intron length increases oscillatory periods of gene expression in animal cells. *Genes Dev.* 22, 2342-2346. doi:10.1101/gad.1696108

Takashima, Y., Ohtsuka, T., González, A., Miyachi, H. and Kageyama, R. (2011). Intronic delay is essential for oscillatory expression in the segmentation clock. *Proc. Natl. Acad. Sci. USA* 108, 3300-3305. doi:10.1073/pnas.1014418108

Webb, A. B., Lengyel, I. M., Jörg, D. J., Valentin, G., Jülicher, F., Morelli, L. G. and Oates, A. C. (2016). Persistence, period and precision of autonomous cellular oscillators from the zebrafish segmentation clock. *eLife* 5, e08438. doi:10. 7554/eLife.08438

Yoshioka-Kobayashi, K., Matsumiya, M., Niino, Y., Isomura, A., Kori, H., Miyawaki, A. and Kageyama, R. (2020). Control of coupling delay for synchronized oscillations in the segmentation clock. *Nature* (in press). doi:10. 1038/s41586-019-1882-z

Yu, X., Alder, J. K., Chun, J. H., Friedman, A. D., Heimfeld, S., Cheng, L. and Civin, C. I. (2006). HES1 inhibits cycling of hematopoietic progenitor cells via DNA binding. *Stem Cells* 24, 876-888. doi:10.1634/stemcells.2005-0598